Supporting Information

Fluorescence detection of Mn^{2+}, $Cr_2O_7^{2-}$ and nitroexplosives and photocatalytic degradation of methyl violet and Rhodamine based on two stable metal-organic frameworks

Yu Wu[a]*, Jian Wu[b], Zhidong Luo[c], Jun Wang[a], Yulong Li[a], Yaoyao Han[c], Jianqiang Liu[c*]

IR spectra

IR spectra of MOFs **1** and **2** displayed the characteristic asymmetric and symmetric stretching vibrations of carboxylate groups in the ranges from 1616 to 1498 cm^{-1}, and from 1599 to 1428 cm^{-1}, respectively. The disappearance of strong absorption bands around 1700 cm^{-1} confirms complete deprotonation of the carboxylate groups of the H_2dbp ligands during the reactions (Fig. S1).

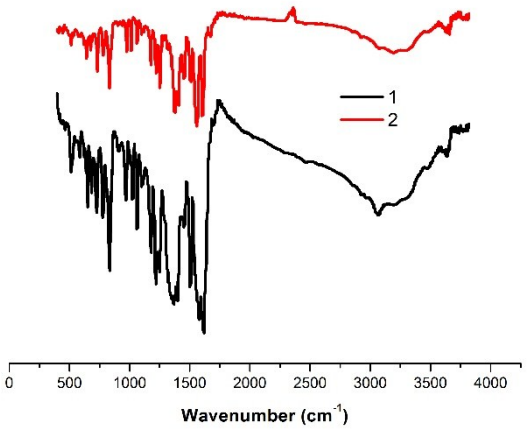

Fig. S1 view of the IR spectra of **1-2**.

Thermogravimetric Analysis (TGA)

The thermogravimetric analyses (TGA) of title MOFs were examined (Fig. S2). In the case of **2** the first weight loss begins at 25°C and is completed at 110 °C. The observed weight loss of 12.2 % corresponds to the loss of the CH_3CN and H_2O molecules (calcd 12.9 %). The second weight loss can be attributed to the elimination of organic ligand. The TGA results indicates that the framework of both **1** and **2** began to collapse only at temperature above 350 °C.

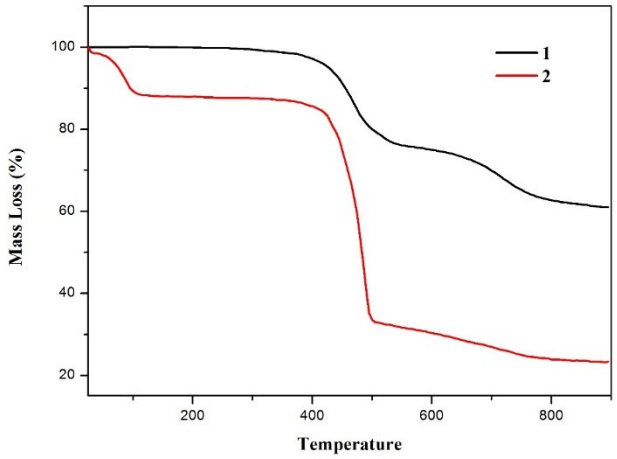

Fig. S2 view of the TGA of **1-2**.

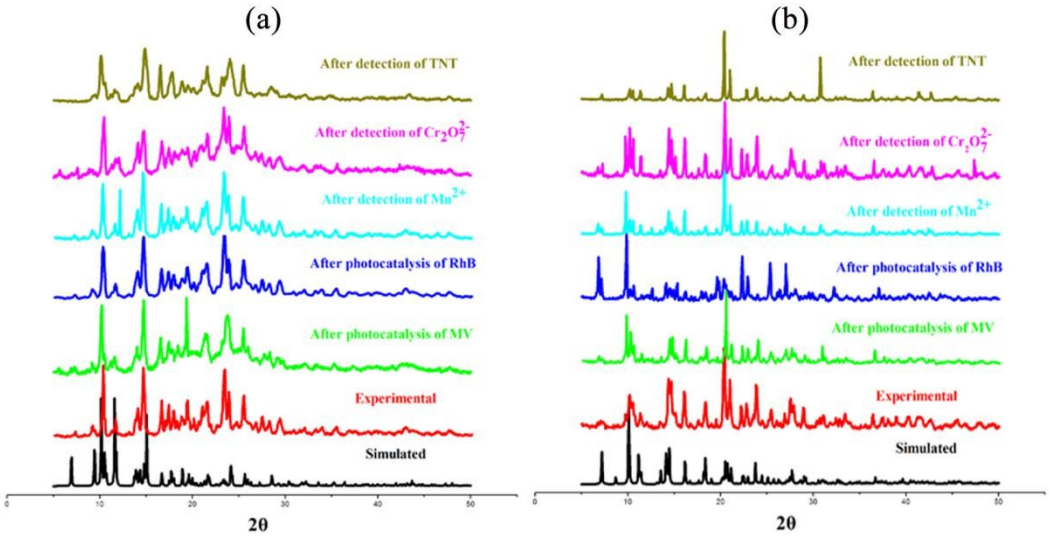

Fig. S3 (a) and (b) Powder XRD profiles of **1-2** after fluorescence sensing and photocatalysis, respectively.

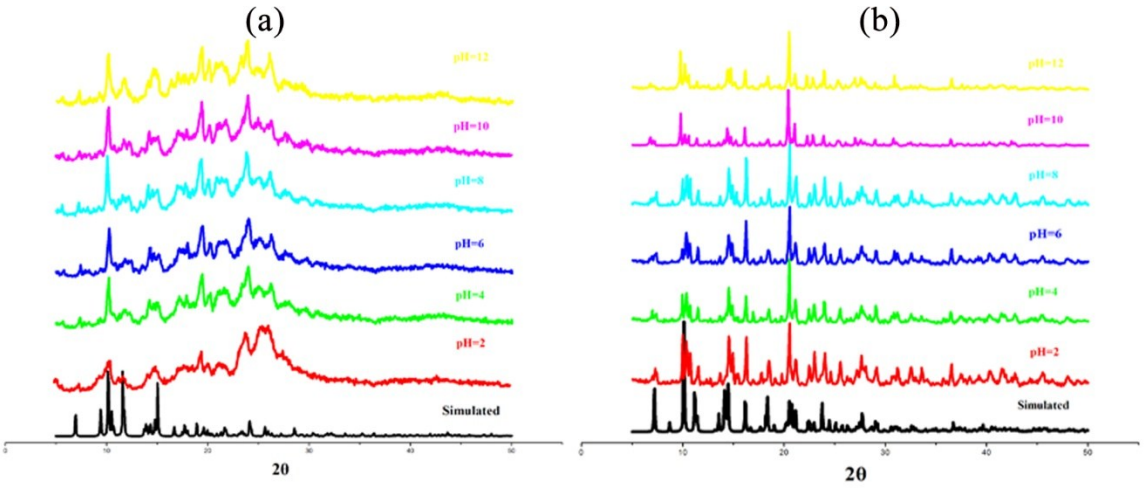

Fig. S4 (a) and (b) Powder XRD profiles of **1-2** under different pH, respectively.

Measurements

The activated samples were prepared by soaking the as-synthesized samples in CH_3OH for two days, then in CH_2Cl_2 for three days and subsequent heating at 100 ºC in a quartz tube under high vacuum for 20 h to remove the solvent molecules prior to measurements. The nitrogen adsorption-desorption measurements were carried out at liquid nitrogen temperature (77 K) by using automatic volumetric adsorption equipment (Micromeritics, ASAP2020).

The desorption hysteresis is related to the 1D narrow channel system, which hints the escape of adsorbed gas molecules. The saturated loading is 77 and 15 cm^3 (STP) g^{-1} at around 700 Torr for **1** and **2**, respctively. The low N_2 adsorbed capacity for **1-2** indicated that the interpenetration greatly reduces the volume of the channel. Also, the differnce loading can be attributed to the skelton of full networks between **1** and **2**.

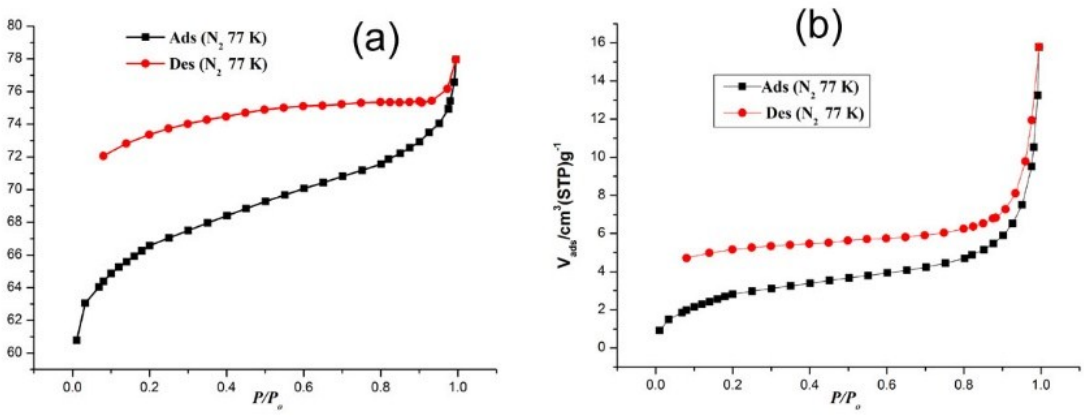

Fig. S5 (a) and (b) Gas sorption isotherms of N_2 (77 K) for **1** and **2**, respectively.

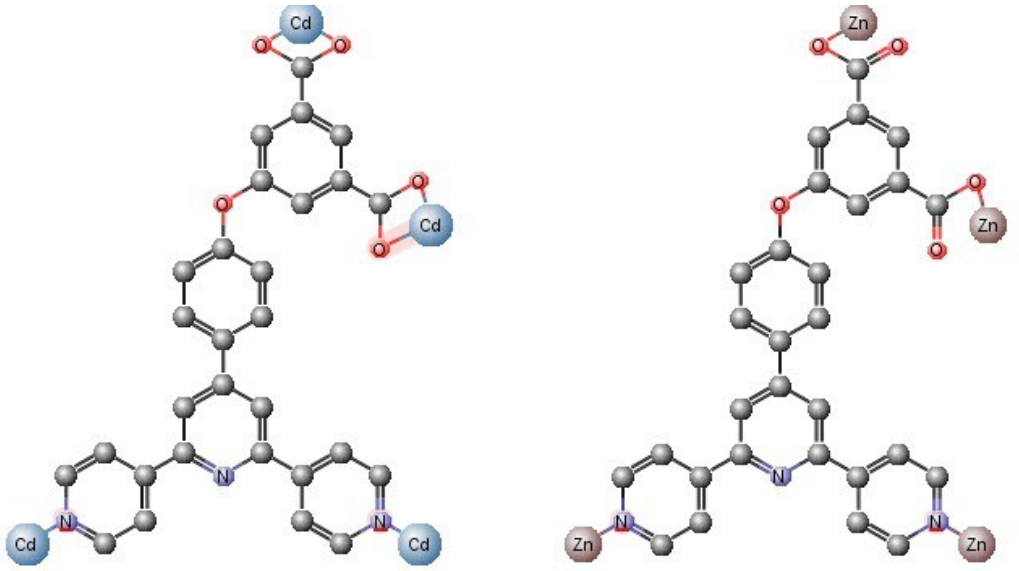

Scheme S1 View of the coordination modes of dbp in this work.

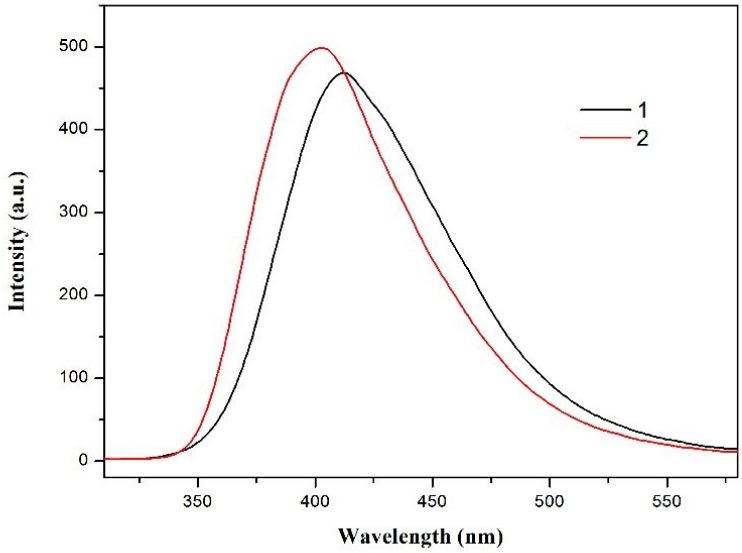

Fig. S6 View of the PL spectra of **1-2** (λ_{ex} = 315 nm).

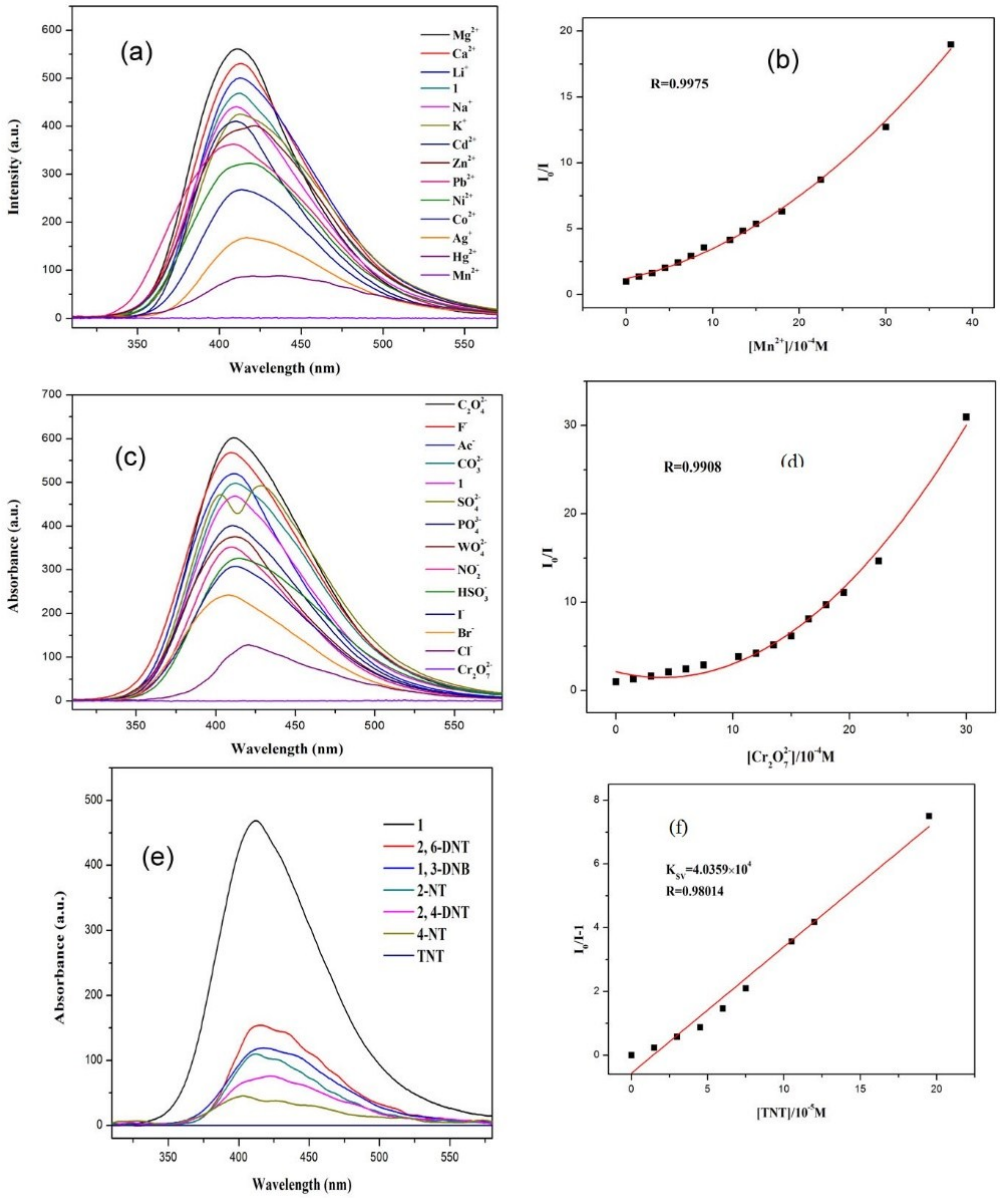

Fig. S7. a), c) and e) Emission spectra of **1** in different metal ions, anions and nitro-explosives (excited at 315 nm). b), d) and f) views of Stern–Volmer plots.

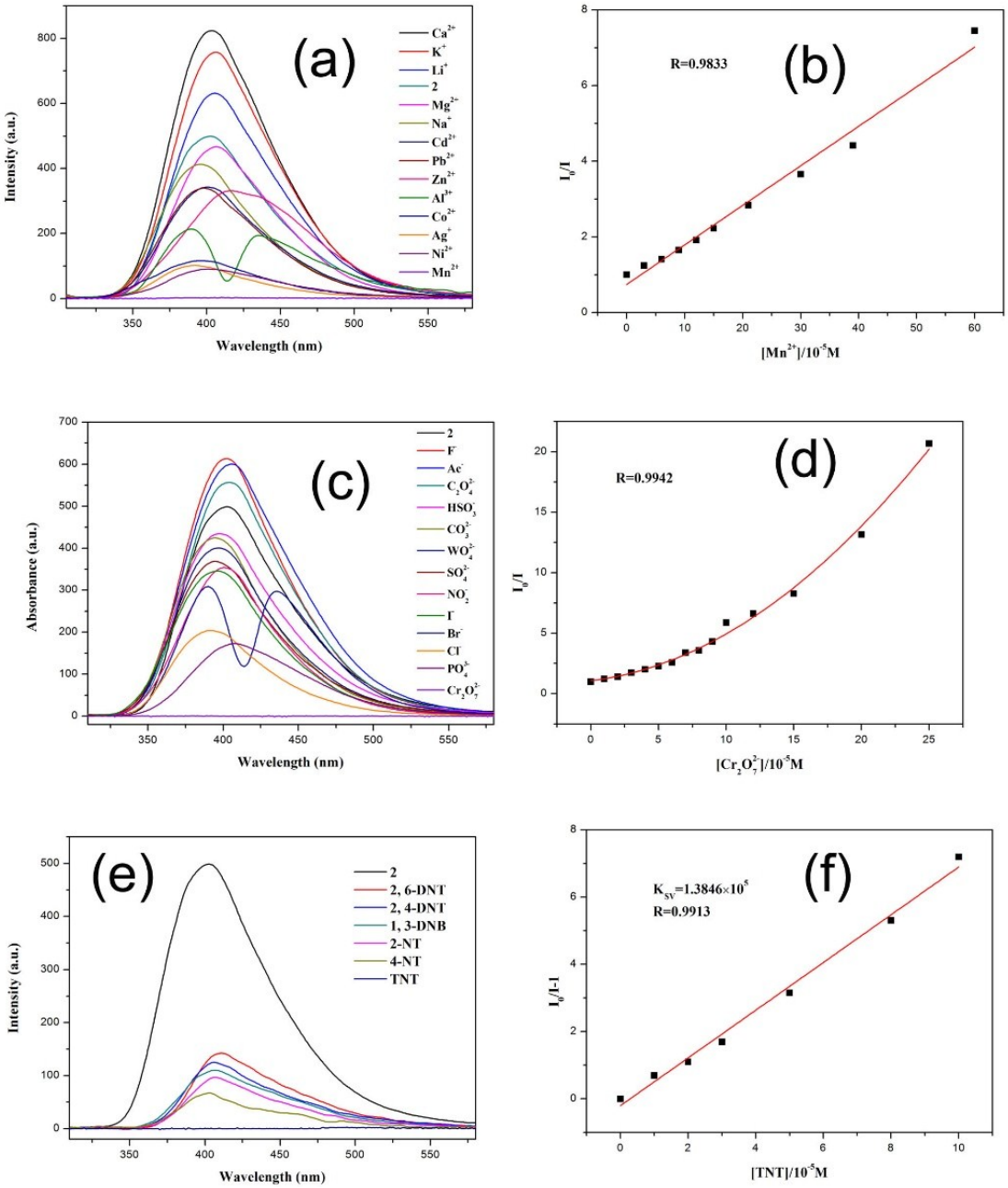

Fig. S8. a), c) and e) Emission spectra of **2** in different metal ions, anions and nitro-explosives (excited at 315 nm). b), d) and f) views of Stern–Volmer plots.

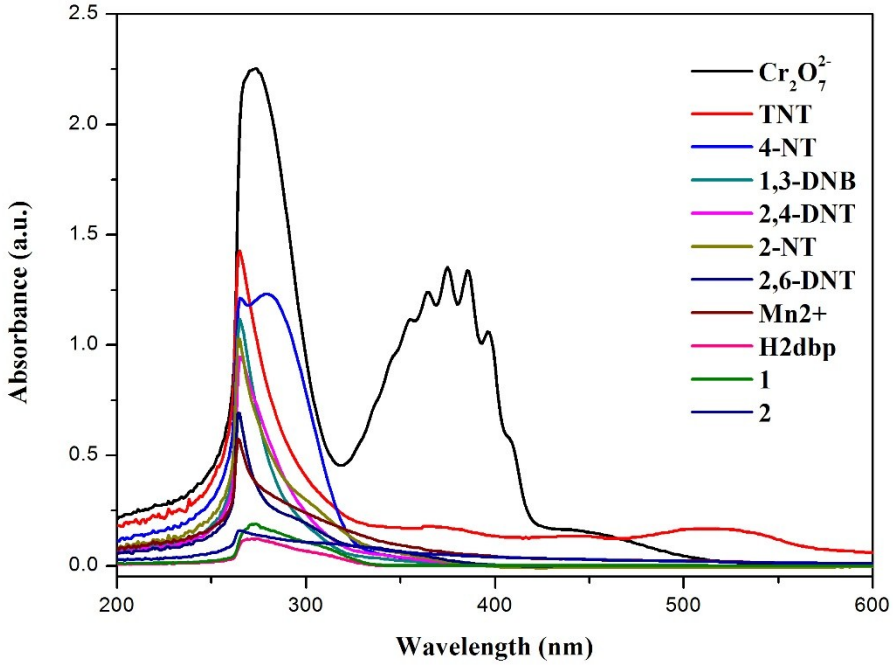

Fig. S9 The UV/vis absorption spectra for Mn^{2+}, $Cr_2O_7^{2-}$, nitro-explosives and dbp.

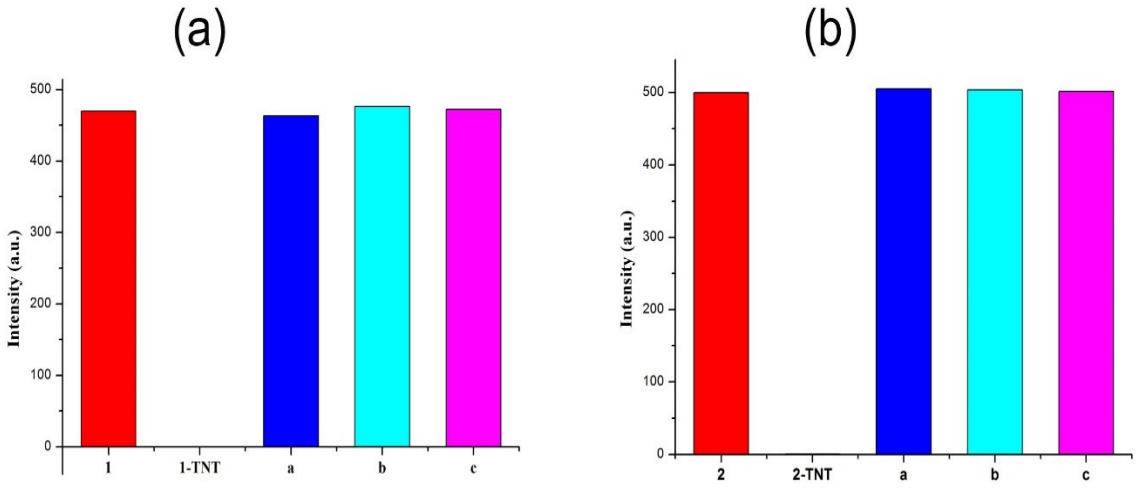

Fig. S10. The luminescence intensity of three recycles (a) after the first recycle, (b) after the second recycle, and (c) after the third recycle in **1-2**.

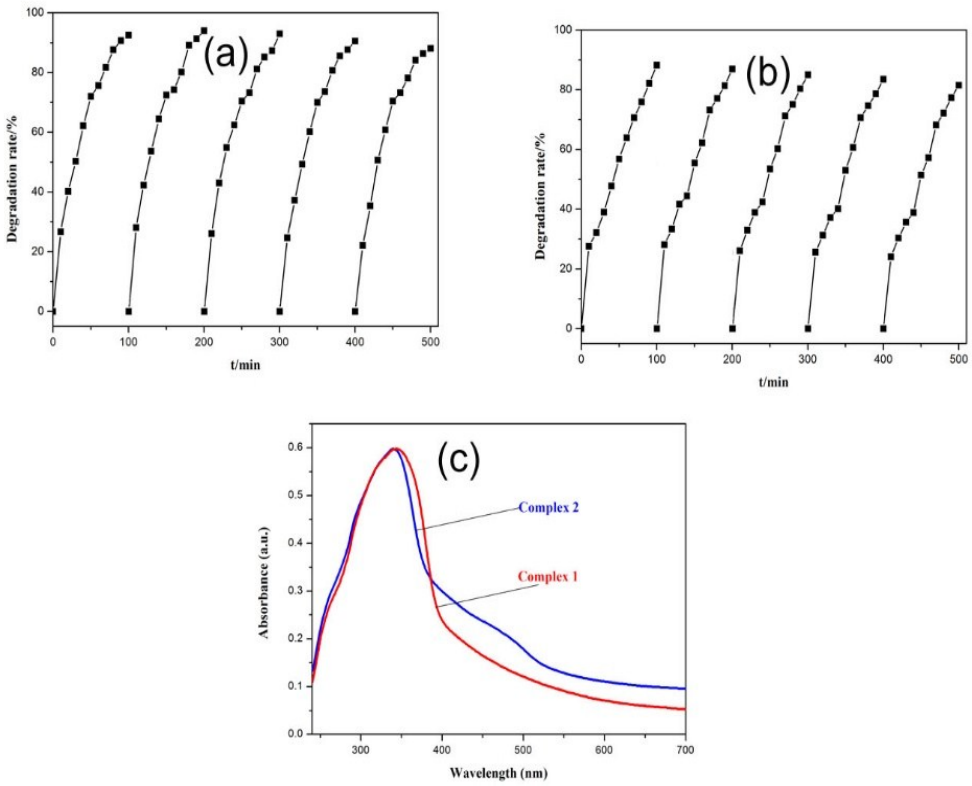

Fig. S11 (a) and (b) recycling tests of **2** towards MV and RhB photodegradation, respectively; (c) view of the UV-vis-NIR.

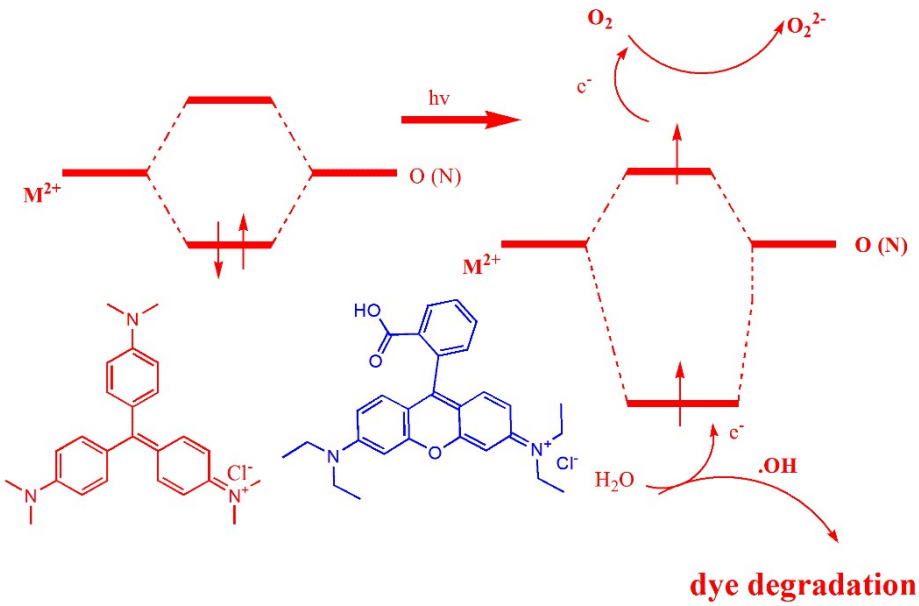

Scheme S2 Schematic of possible photocatalytic reaction mechanism of MV and Rh

B.

Table S1. Crystal data and structure refinement information for compounds **1**and **2**

Parameter	**1**	**2**
Formula	$C_{29}H_{17}ZnN_3O_5$	$C_{62}H_{52}Cd_2N_8O_{16}$
Formula weight	552.83	1389.92
Crystal system	Monoclinic	Monoclinic
Space group	P21/c	P21/c
Crystal color	yellow	yellow
a, [Å]	9.413(2)	10.1676(16)
b, [Å]	18.749(5)	17.300(3)
c, [Å]	17.387(5)	17.485(3)
α, [°]	90.00	90
β, [°]	91.076(4)	91.708(2)
γ, [°]	90.00	90
V, Å ^{3}	3067.9(14)	3074.3(9)
Z	4	2
ρ_{calcd}, g/cm^3	1.197	1.501
μ, mm^{-1}	0.838	0.767
F(000)	1128	1408
θ Range, deg	2.42–25.01	2.35–25.01
Reflection collected	5391/3904	15377/5413
Goodness-of-fit on F^2	1.062	1.051
R_1, $wR_2(I> 2\sigma(I))^*$	0.0759, 0.0996	0.0359, 0.0465
R_1, wR_2 (all data)**	0.1901, 0.1992	0.0951, 0.1004

* $R = \sum(F_o - F_c)/\sum(F_o)$, ** $wR_2 = \{\sum[w(F_o^2 - F_c^2)^2]/\sum(F_o^2)^2\}^{1/2}$.

Table S2. Selected bond distances (Å) and angles (°) of structures **1-2**

1

Zn(1)-O(2)#1	1.951(4)	Zn(1)-O(4)#2	1.954(4)
Zn(1)-N(3)#3	2.030(5)	Zn(1)-N(1)	2.051(4)
O(2)#1-Zn(1)-O(4)#2	115.85(17)	O(2)#1-Zn(1)-N(3)#3	101.19(19)
O(4)#2-Zn(1)-N(3)#3	116.76(19)	O(2)#1-Zn(1)-N(1)	120.7(2)
O(4)#2-Zn(1)-N(1)	95.72(18)	N(3)#3-Zn(1)-N(1)	107.4(2)

Symmetry codes: #1: -1+x, y, -1+z; #2: x, y, -1+z; #3:1-x, 0.5+y, 0.5-z

2

Cd(1)-O(1)W	2.309(3)	Cd(1)-O(2)#1	2.312(2)
Cd(1)-N(1)	2.317(3)	Cd(1)-O(4)#2	2.331(2)
Cd(1)-N(3)#3	2.356(3)	Cd(1)-O(3)#2	2.513(3)
Cd(1)-O(1)#1	2.634(2)		
O(1)W-Cd(1)-O(2)#1	86.18(9)	O(1)W-Cd(1)-N(1)	90.82(10)
N(1)-Cd(1)-O(2)#1	139.04(9)	O(1)W-Cd(1)-O(4)#2	91.15(10)
O(2)#1-Cd(1)-O(4)#2	84.95(9)	O(1)#1-Cd(1)-O(3)#2	166.77(8)
N(3)#3-Cd(1)-O(1)#1	80.94(10)	O(4)#2-Cd(1)-O(1)#1	137.16(8)
N(1)-Cd(1)-O(1)#1	86.83(9)	O(1)W-Cd(1)-O(1)#1	89.27(9)
N(3)#3-Cd(1)-O(3)#2	107.43(10)	O(4)#2-Cd(1)-O(3)#2	53.94(8)

Symmetry codes: #1: 1+x, y, 1+z; #2: x, y, 1+z; #3: 4-x, -0.5+y, 1.5-z